Quantum chemical cluster study of hydrated halide adsorption on the cathodic Al(111) surface

ARTICLE *in* SURFACE SCIENCE · OCTOBER 1999

Impact Factor: 1.93 · DOI: 10.1016/S0039-6028(99)00793-1

2 AUTHORS, INCLUDING:

Visvaldas Kairys
Vilnius University
47 PUBLICATIONS **1,121** CITATIONS

SEE PROFILE

ELSEVIER

Surface Science 440 (1999) 169–186

surface science

www.elsevier.nl/locate/susc

A quantum chemical cluster study of hydrated halide adsorption on the cathodic Al(111) surface

Visvaldas Kairys[1], John D. Head *

Department of Chemistry, University of Hawaii, 2545 The Mall, Honolulu, HI 96822, USA

Received 16 April 1999; accepted for publication 28 June 1999

Abstract

Ab-initio cluster calculations are used to simulate water, fluorine and iodine adsorption on a negatively charged Al(111) surface. In contrast to our earlier work using neutral Al clusters, we determine the water to be only weakly adsorbed above the negatively charged Al clusters, with the water H atoms being closest to the metal surface. A H-bond network is readily formed when more than one water molecule is adsorbed on the Al cluster surface. Analogous to the recent in-situ surface X-ray scattering experiments on Ag(111) surfaces, we find the separation between the water and the cathodic surface to be approximately 1.5 times greater than that found previously for the neutral Al(111) surface. In addition, there is a strong repulsion preventing the water molecules from being closer than 3.0 Å to the negatively charged surface. For the halides, in line with gas-phase adsorption experiments and other calculations, we find that fluorine is much more strongly bound to the Al clusters than iodine, with the Al(111) atop site being the most favored surface site for both halides. By performing calculations on Al clusters with a halide ion and one or more water molecules coadsorbed, we are able to develop an explanation as to why solvated iodine is more readily able to specifically adsorb on a cathodic surface than fluorine. The larger atomic size of iodine enables it to adsorb on the cathodic Al(111) surface at a higher vertical height than fluorine. Water molecules can then bond to iodine without being drawn into the region of repulsive interaction from the negatively charged surface. Thus we find the adsorption energy for $I^- \cdot (H_2O)_3$ adsorbed on Al_{19}^- to be very similar to the I^- adsorption energy, suggesting that iodine can be specifically adsorbed on the cathodic Al(111) surface without destabilizing any coadsorbed water molecules, whereas any water molecules hydrogen-bonding to fluorine are pulled towards the Al(111) surface and destabilized when the fluorine atom is also bonded to a surface Al atom. As a consequence, even though we find for the clusters with $F^- \cdot (H_2O)_3$ adsorbed on Al_{19}^- that the Al—F bond is still formed, the calculations show the Al—F bond to be now severely strained.

Keywords: Ab initio cluster calculations; Al(111) surface; Chemisorption; Electrochemistry; Halide adsorption; Water adsorption

1. Introduction

Recent in situ experiments have provided powerful new insights into the microscopic interactions taking place at electrode surfaces. Prior to this work, experimental investigations of water adsorption on metal surfaces under ultra high vacuum (UHV) conditions using a variety of surface science techniques has led to a model in which water forms a hexagonal ice-like structure on metal surfaces [1,2]. The first water layer next to the neutral or positively charged surface has the water O atoms closest or "pointing towards" to the

* Corresponding author. Fax: +1-808-956-5908.

E-mail address: johnh@gold.chem.hawaii.edu (J.D. Head)

[1] Present address: Department of Chemistry, University of Iowa, 305 Chemistry Building, Iowa City, IA 52242-1294, USA.

0039-6028/99/$ – see front matter
PII: S0039-6028(99)00793-1

metal surface. The hexagonal ice lattice-like structure is formed when water in the second and higher adsorbate layers H-bond to water molecules in the preceding layers. Molecular dynamics calculations readily simulated the water layering structure required by the ice-like model for water close to an electrode [3–7]. On negatively charged cathodic metal surfaces, the water direction is expected to be reversed, with the O pointing away and the H atom closest to the surface. Toney et al.[8] inferred this structure at a cathodic Ag(111) electrode by using in situ surface X-ray scattering (SXS) experiments to measure the water distribution perpendicular to the electrode surface. Only the positions of the O atoms were measured, and they found the water to be ordered into at least three layers above the metal surface. On the positively charged Ag(111) surface, the O atom distribution has a leading edge at 1.95 Å and a fairly broad peak at 2.7 Å above the surface, while on the cathodic Ag(111) surface the leading O edge is at 3.05 Å and has a much sharper peak in the O height distribution at 3.7 Å. Toney et al. argue that the much longer O to cathodic Ag(111) surface distance is consistent with the water O atom pointing away from a negatively charged surface. Unexpectedly, the SXS experiments showed the first water layers to contain $1.55\times\ 10^{15}$ and 2.6×10^{15} water molecules per cm^2 on the negatively and positively charged surfaces, respectively. These surface coverages are considerably higher than the 1.15×10^{15} water molecules per cm^2 expected from the bulk water density. Berkowitz et al. [7], using molecular dynamics calculations to simulate water between Ag(111) electrodes, also found water layer structures with the first layer having a water dipole direction consistent with the surface charge . However, Berkowitz et al. only computed a maximum of 1.78×10^{15} water molecules per cm^2 on the neutral Ag(111) surface, and found this coverage to decrease on more positively charged electrodes. These computed water coverages will be sensitive to the water–metal interaction potential used in the molecular dynamics simulations. Ataka et al. [9], using in situ surface-enhanced infrared absorption spectroscopy (SEIRAS) on electrolytes at an Au(111) electrode also observed a reordering of the first surface water layer as the electrode potential was changed. They concluded that water has an ice-like structure with the O atom closest to the metal on the positively charged surface, the structure reversing on the negatively charged surface with the H atoms being closest to the surface. The structures of Ataka et al. are based on their interpretation of vibrational spectral data, and do not provide any direct geometric parameters for the interface.

Another important aspect of the microscopic structure of electrodes involves the specific adsorption of anions on these surfaces. In their SEIRAS experiments, Ataka et al. [9] found the water ice-like structure on more positive electrodes to be broken by the specific adsorption of either the perchlorate or sulfate ion from the electrolyte. For the halides, it is well known that the greater the anion size, the more strongly the halide specifically adsorbs, even on cathodic surfaces [10]. Recent in situ scanning tunneling microscopy (STM) and atomic force microscopy (AFM) experiments have resolved ordered iodide structures on a number of negatively charged metal electrodes [11–14]. The fluoride ion, on the other hand, shows very little tendency to specifically adsorb on even positively charged electrode surfaces, suggesting that it has a much weaker interaction than iodide with metal surfaces. However, in agreement with the expectations from gas-phase halide adsorption experiments [15], quantum chemical calculations on metal clusters find fluorine to be much more strongly adsorbed than iodine on metal surfaces [16–21]. Of course, these studies are in the absence of water and do not take into account solvation effects. The -113.3 kcal mol^{-1} F^- enthalpy of solvation versus -64.1 kcal mol^{-1} for I^- greatly favors F^- staying in solution [22]. Nonetheless, a good explanation at the atomic level as to why I^- is so strongly specifically adsorbed on cathodic surfaces is still lacking.

The aim of the present work is to explore some of the fundamental interactions taking place in water, fluorine and iodine adsorption and halide/water coadsorption on a negatively charged Al(111) surface using quantum chemical cluster calculations. Our calculations provide an alternative to the approximate adsorbate–metal interaction potentials which are currently used in

molecular dynamics simulations [3–6]. One reason why we chose to work with an Al surface was because we have previously performed cluster calculations which simulated water adsorption on the neutral Al(111) surface [23,24]. The cluster method takes advantage of the feature that chemisorption interactions are often predominantly localized on the adsorbate and a few nearby metal atoms. The cluster method models a metal surface by using a cluster of atoms having the same arrangement and geometry as the extended surface. Then, the properties of adsorption are determined by performing standard quantum chemistry calculations on the adcluster formed from the adsorbate and the metal cluster. The experience of many workers is that adsorbate geometries and vibrational frequencies converge rapidly with cluster size, but adsorption energetics are more problematic [25,26]. In our calculations with one and two water molecules adsorbed on a variety of neutral Al clusters we obtained structures consistent with the formation of the ice-like lattice with the water O atom being closest to the metal surface and preferentially adsorbed approximately 2.0 Å vertically above an Al atop site [23,24]. Other ab initio calculations on neutral clusters have found that the water O atom is closest to Hg [27,28] and Ni [29] surfaces. One way to use cluster calculations to model a charged surface is to apply an external uniform electric field across the cluster and adsorbate [30]. Sellers et al. [27], in their work on neutral Hg clusters, speculated that the application of such an electric field might cause the orientation of the water molecule to be reversed, with the H atoms closer to the metal surface. An alternative approach, which we use in the present work, is to simply add or remove electrons from the system so that the cluster has an overall net charge. This approach has the disadvantage of introducing discontinuous jumps in the surface charge as the number of electrons is increased. These surface charge jumps are obviously cluster-size dependent, and in order to simulate realistically a negatively charged metal surface and its resultant electric field, we anticipated that it is necessary to perform calculations on clusters which have relatively large surface areas. Thus, a second reason for investigating the cathodic Al(111) surface is that we can more readily perform quantum chemical calculations on large Al clusters than on clusters of transition-metal atoms, which are the more traditional components on an electrode.

The remainder of the paper is organized as follows. In the Section 2 the Al clusters and computational methods are described. Our results and a discussion are presented in the Section 3, which is subdivided into three parts. Section 3.1 describes the interaction of water molecules only with the cathodic Al(111) surface, and shows the O atom in the water molecule to point away from the metal surface. Section 3.2 presents results for the adsorption of a single fluoride and iodide ion alone on differently charged Al clusters, and demonstrates that fluorine interacts much more strongly than iodine with the Al(111) surface. Section 3.3 discusses the results from fluoride/water and iodide/water coadsorption on Al clusters, and provides some insight into why I^- specifically adsorbs more readily than F^- on a cathodic metal surface. Some concluding remarks are given in the Section 4.

2. Method

The cluster method is used to model water, fluorine and iodine adsorption and coadsorption on the cathodic Al(111) surface. The Al(111) surface was approximated by single-layer Al_7, Al_{12} and Al_{19} and double-layer Al_{18}(12,6), Al_{19}(12,7) and Al_{31}(19,12) clusters having the same geometries as fragments of the bulk Al fcc lattice with a 2.8635 Å Al–Al internuclear distance [31]. For the two-layer clusters we use the common notation of specifying in parenthesis the number of Al atoms in each surface layer. The Al_7 cluster has a central Al atom surrounded by its complete shell of Al nearest-neighbors from the top Al(111) surface layer, while Al_{12} consists of a central triangle of three surface Al atoms surrounded by the next complete shell of Al nearest-neighbors from the top surface layer, and the Al_{19} cluster is formed by surrounding the Al_7 cluster by its next shell of Al nearest-neighbors. The Al_{18}(12,6) and Al_{19}(12,7) clusters again consist of a central triangle of surface Al atoms, but they are now sur-

rounded by all of the Al nearest-neighbors from both the top and second Al(111) surface layers. Because of the layer stacking in the Al fcc bulk lattice, the $Al_{18}(12,6)$ cluster has an fcc or open three-fold site at its center, while the $Al_{19}(12,7)$ cluster has the hcp or eclipsed three-fold site at its center. Similarly, $Al_{31}(19,12)$ contains the Al_7 cluster in the surface layer surrounded by all the Al nearest-neighbors from the top two Al(111) surface layers. The cathodic Al(111) surface was simulated by performing calculations on the above clusters but with a sufficient number of electrons, so that the adcluster has an overall negative charge.

We determine the adsorbate equilibrium geometry by minimizing the adcluster energy while keeping all the Al cluster atoms at their bulk-like positions. The different adcluster-restricted closed and open-shell energies were computed at either Hartree–Fock (HF) or second-order Moller–Plesset perturbation theory (MP2) levels. The restricted open-shell MP2 (ROMP2) calculations use the formalism developed by the groups of Bartlett and Handy [32,33]. Most of the equilibrium adsorbate geometries described in Section 3 were obtained by minimizing the adcluster HF energy using two main methods. When the adsorbate consists of more than one atom we perform an energy-derivative based partial geometry optimization [34]. The adsorbate is free, apart from any intrinsic symmetry constraints, to move across the cluster surface over different types of adsorption sites until it adopts a geometry with the lowest energy. Alternatively, for a single-atom adsorbate, such as the halogens, we determine equilibrium geometries at a specific adsorption site by minimizing the adcluster energy along a fixed direction normal to the surface site. This second procedure allows us to compare the relative energies for adsorption at different types of surface site. Finally, to evaluate whether the adsorbate geometries obtained at the HF level are not drastically changed when electron correlation is introduced, we optimized water vertical heights above the Al surface by starting with the HF equilibrium geometry of the adcluster and translated the water molecule perpendicular to the surface until a minimum in the MP2 energy was obtained.

All of the geometry optimizations and energy calculations were performed with the GAMESS program [35], usually with direct methods and in parallel at the Maui High Performance Computing Center. The Hay–Wadt effective core potentials and split valence basis sets containing three and seven valence electrons, respectively, were used for Al and I [36]. The Dunning–Hay basis set were used for H, O and F [37]. The O basis was augmented with a diffuse p (exponent 0.059) and d (0.85) polarization functions [37]. The F basis was augmented with diffuse sp (0.1076) [38] and d (0.90) polarization functions [37]. Similarly, the I basis was augmented with diffuse sp (0.0368) and d (0.266) polarization functions [38].

Previous work by ourselves and others has shown that adsorbate geometries generally converge well with cluster size and type [25,26,39–42]. Unfortunately, adsorption energies tend to exhibit erratic convergence behavior with different clusters, making the theoretical determination of the preferred adsorption site for an adsorbate difficult. One approach is to compare the cluster total energies computed for the optimized adsorbate geometries at each of the different adsorption sites all on the same cluster. Thus calculations with the $Al_{18}(12,6)$ cluster enable the relative energies E_r for adsorption at the atop, bridging and three-fold fcc sites to be compared. However, this does not facilitate a reliable comparison of the energies for adsorption at the two different three-fold site types present in the $Al_{18}(12,6)$ and $Al_{19}(12,7)$ clusters. An alternative approach, which has been used by several other groups [19,20,43,44], is to define an adsorption energy AE for the adsorbate Y^q by

$$AE(Y^q) = -[E(\mathrm{Al}_n Y^{p+q}) - E(Y^q) - E^*(\mathrm{Al}_n^p)], \quad (1)$$

where $E(\mathrm{Al}_n Y^{p+q})$ is the energy of the adcluster with charge $p+q$, $E(Y^q)$ is the energy of the free adsorbate Y with charge q, and $E^*(\mathrm{Al}_n^p)$ is the energy of naked a Al_n^p cluster with charge p, with the asterisk denoting that the electronic state of the naked cluster should correspond to a properly prepared bonding state [39–42]. Many of the low-lying excited electronic states for the naked cluster would be expected to be degenerate if the cluster had an infinite surface. The properly prepared bonding state of a naked cluster can be defined as

the same electronic state which the substrate atoms adopt in the adcluster to favor forming a strong adsorbate interaction. Adsorption at different surface sites on the cluster may require different prepared states for the naked cluster. In the case of halide-ion adsorption, since it is isoelectronic with an inert gas, it contributes a totally symmetric closed shell to the adcluster, requiring the total symmetry for the electronic states of the naked cluster and the adcluster to be identical. This is accomplished by requiring the sum of the different irreducible representations in the naked cluster and the adsorbate electronic configurations to equal those in the electron configuration of the adcluster. One disadvantage of computing the adsorption energy with Eq. (1) will be the presence of a Coulombic term pq/D, with D being some effective distance between the adsorbate and naked cluster charges. This Coulombic term will prevent simple comparisons between adsorption energies from different clusters. In Section 3 we use both the relative energy E_r and adsorption energies AE to compare the adsorption at different surface sites. To avoid later confusion, it is worth noting that when an adsorption site has a positive relative energy E_r, it is less stable than a site with zero energy, whereas the adsorption energy AE, defined by Eq. (1), increases when the adsorption site is more stable.

3. Results and discussion

3.1. Water adsorption on negatively charged Al clusters

We have modeled the interaction of water with the cathodic Al(111) surface using several single- and double-layered negatively charged clusters of Al atoms. In prior work, we have investigated the adsorption of water on various neutral Al clusters to simulate the neutral Al(111) surface [23,24]. A typical example of the adsorption geometry determined for two water molecules on the neutral surface is shown in Fig. 1. One of the water molecules interacts directly with the Al surface through the oxygen atom 2.0 Å vertically above the atop site. We computed the water adsorption

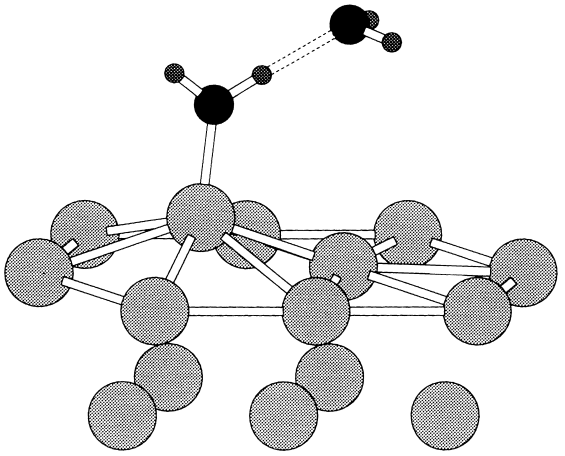

Fig. 1. Typical water adsorption structure obtained with neutral clusters modeling the Al(111) surface [23,24]. This is the lowest-energy structure determined in the partial geometry optimization of the two water molecules and the two central Al atoms in the Al_{15}(10,5) cluster. The water closest to the Al(111) surface is adsorbed 2.0 Å above an atop site, while the second water hydrogen bonds to the first water to give a structure prototypical of the formation of a water bilayer. Optimized structures involving hydrogen bonding between the water molecules are produced even in calculations where the initial geometry has both water molecules at neighboring atop sites.

energies to be in the 15–20 kcal mol^{-1} range. The second water molecule hydrogen bonds to the first water and forms a structure which is prototypical of the formation of a water bilayer on the Al(111) surface. The character of the water–surface interaction changes dramatically on the negatively charged Al(111) surface. In all of our calculations on the different negatively charged clusters we find that the water direction is reversed, with the hydrogen atoms being closer to the surface. A representative water structure is illustrated in Fig. 2 for the Al_{31}^{-}(19,12) cluster, although our calculations find the water adsorption energy to be essentially site independent. Table 1 lists water adsorption energies and optimized water–surface nearest distances computed for different negatively charged Al clusters. At the HF level, the water adsorption energy to the negatively charged clusters is only 3–5 kcal mol^{-1} and the minimum distance between the water molecule and the negative charged Al cluster increases to more than 1.5 times that found for the neutral clusters. However,

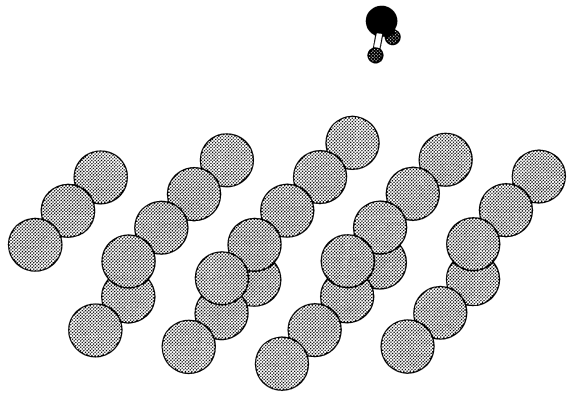

Fig. 2. Optimized structure for water adsorbed on the cathodic $Al_{31}^{-}(19,12)$ cluster. For all the negatively charged Al clusters we find the water orientation to be reversed with respect to that found on the neutral Al clusters. In the $Al_{31}(19,12)H_2^{-}O$ partial optimization, the water moves to the bridge site shown. The same basic bridge structure, apart from a slightly higher vertical height, is also obtained for the single-layer Al_{19}^{-} cluster. However, the energetic distinctions for water adsorption at other types of surface sites is less than 1 kcal mol^{-1}.

Table 1
Water adsorption energies (kcal mol^{-1}) and geometries (Å) obtained with various negatively charged Al cluster: the water molecule is optimized above the center of the cluster surface, and lateral translations of the water molecule towards different adsorption sites typically change the adsorption energy by less than 1 kcal mol^{-1}. The oxygen atom surface height is 0.6 Å longer than the H surface height

	HF		MP2	
	AE	H height	*AE*	H height
Al_7^-	4	3.85	6	3.42
Al_{12}^-	4	3.85	5	3.14
$Al_{18}(12,6)^-$	4	3.59	7	3.05
$Al_{19}(12,7)^-$	4	3.49		
Al_{19}^-	3	3.86	4	3.65
Al_{19}^{-2}	5	3.99	5	3.99
$Al_{31}(19,12)^-$	3	3.73	7	2.93
$Al_{31}(19,12)^{-2}$	5	3.68	9	3.07
$Al_{31}(19,12)^{-3}$	7	3.67	11	3.12
$Al_{31}(19,12)^{-4}$	9	3.64	13	3.13

unlike neutral Al clusters and adsorbate geometries in general on clusters, we find the distances from water to the negatively charged Al clusters to be more sensitive to the cluster type. The water vertical heights listed in Table 1 were obtained from partial geometry optimizations, which find the lowest-energy structure for the water without any restriction on the preferred adsorption site. Somewhat different and longer vertical heights are obtained when water adsorption is restricted to specific three-fold, atop or bridge sites on the Al(111) surface, but the HF water adsorption energies still remain in the 3–5 kcal mol^{-1} range. At the HF level, we find H heights between 3.85 and 4.00 Å for the single-layer negatively charged Al clusters, and slightly shorter (3.45–3.75 Å) H heights on the two-layer clusters. This relatively broad range in the vertical heights is probably because of the small water binding energies, but could also be a consequence of variations in the surface charge distributions on the different clusters. Interestingly, the results from both Mulliken and Löwdin population analyses show the surface atoms on the negatively charged clusters to exhibit smaller charge variations than in the neutral clusters. This charge smoothing arises from SCF orbital relaxation effects caused by the addition of the extra electron to the lowest unoccupied molecular orbital. Thus, from the surface charge point of view, negatively charged clusters may be a more realistic of a metal surface than neutral clusters. The MP2 calculations produce somewhat shorter (2.93–4.00 Å) water–Al surface distances and slightly larger (4–9 kcal mol^{-1}) adsorption energies. In the MP2 calculations, the vertical height of water above the surface was optimized by starting with the Hartree–Fock equilibrium geometry of the adcluster and translating the water molecule perpendicular to the Al cluster surface until a minimum in the MP2 energy was obtained. A sum of the Al (2.05 Å) and H (1.2 Å) van der Waals radii [45] suggests that the H–Al surface distance should be around 3.25 Å which is quite close to the distances predicted by the MP2 calculations. There is a slight shortening of the water–surface distance and an increase in the binding energy when the charge on Al_{19} is increased from -1 to -2, presumably due to an increase in the electric field strength. A similar trend is found for the two-layer $Al_{31}(19,12)$ clusters. These different water adsorption geometries on the neutral and negatively charged Al clusters are consistent with the X-ray scattering measurements by Toney et al.

[8], who observed the average O–surface distances for a positively charged and a negatively charged Ag(111) electrode to be 2.7 and 3.7 Å, respectively. We also checked to ensure that the water binding energy was not strongly influenced by a basis-set superposition error by using the Boys counterpoise correction procedure [46] method, but found the adsorption energies to be reduced by less than 0.2 kcal mol^{-1} [47].

The small water adsorption energy, which is independent of the adsorption site, coupled with the relatively large distance between the water and the Al cluster surface, suggests that the binding is mainly due to electrostatic interactions between the water dipole and the electric field generated by the negatively charged Al surface. Some confirmation of the absence of covalent interactions between the water and the cathodic Al(111) surface was found in contour plots of the total HF electron density for the $Al_{19}H_2O^-$ cluster. The Al_{19}^- and water parts of the electron density were only slightly polarized from those found for the bare Al_{19}^- cluster and isolated water [47]. The electrostatic nature of the bonding is further illustrated by the variation of the HF and MP2 water adsorption energies on Al_{19}^- with surface height is shown in Fig. 3. Included in Fig. 3 is a dotted line which represents the electrostatic interaction energy between the electric field and the water dipole moment computed using $E = -\boldsymbol{F}\cdot\mu$, where $\boldsymbol{F}$ is the electric field and μ is the water dipole moment vector. The water dipole moment was taken to be oriented perpendicular to the surface, and thus parallel to the electric field. The electric field strengths $|\boldsymbol{F}|$ at different heights above the naked cluster surface were determined from the Al_{19}^- nuclear and electronic charge distributions and calculated using the GAMESS program. The water dipole moment was taken as 2.28 D. This is the dipole moment computed for a water molecule having the same geometry as in the cluster calculation, but now in the absence of an external electric field. The similarity in the shapes of the water adsorption energy variation obtained from the cluster calculations and the dotted curve simulating the water dipole–electric field interaction is remarkable. The relatively slow convergence of the water adsorption energy to zero at long distances

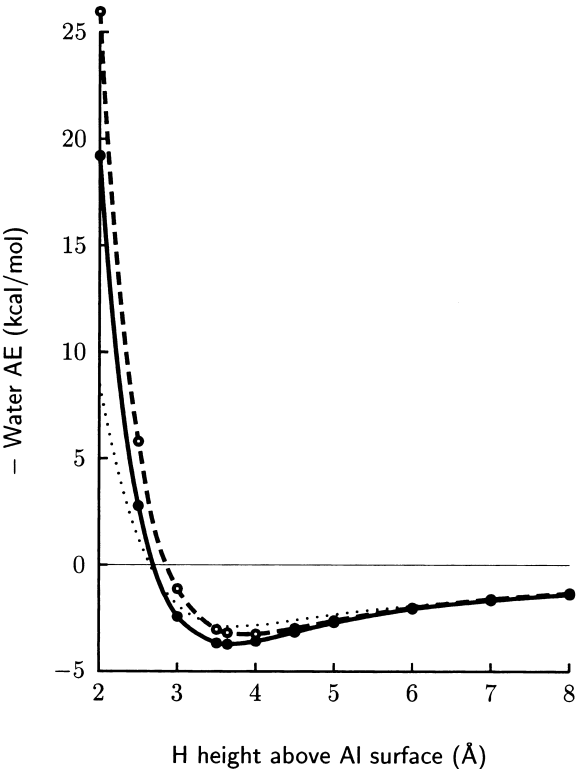

Fig. 3. Variation of water adsorption energy (HF (○) and MP2 (●)) with vertical height above the type of bridging site shown in Fig. 2 for the single layer Al_{19}^- cluster. The dotted line corresponds to the classical electrostatic interaction energy between the constant 2.28 D dipole moment taken from an unpolarized water molecule and the electric field generated from the nuclear and electronic charge distributions on the naked Al_{19}^- cluster.

is also a characteristic of the purely electrostatic interaction. On an infinite surface, the electric field strength would be constant everywhere, causing the dipole–electric field interaction energy to remain constant. In the present work, the slow decay of the water adsorption energy curve is an artifact of the limited size of the Al_{19}^- cluster. Some of the differences between the cluster's water adsorption energy variation and the simulated dipole–field interaction curve will be due to the fact that the polarizability of the water molecule by the charged surface in the simple electrostatic model is ignored.

Although the water adsorption energy is small on the negatively charged clusters, Fig. 3 also shows that a steeply increasing repulsive inter-

action develops between water and Al_{19}^- when their separation is less than 3 Å. Bagus and co-workers [48] have previously pointed out the existence of this type of repulsive surface "wall", which they ascribed to Pauli repulsion arising from the non-bonding overlap of the surface and adsorbate charge distributions. As we discuss further in Section 3.3, it is the water height at which the repulsive wall starts to rapidly increase which has an important controlling effect on whether an anion can specifically adsorb on a cathodic metal surface.

As Fig. 1 illustrates, H-bonding between water molecules becomes important with increasing water coverage on the metal surface. To investigate hydrogen bonding effects on the cathodic Al(111) surface, we partially optimized the geometry for three molecules adsorbed on the Al_{19}^- cluster. Since the water adsorption energy on the cathodic Al(111) surface is small, we again find the water molecules readily form hydrogen bonds with each other to produce the "crown"-type structure shown in Fig. 4 with a ring of water OH bonds having a 2.94 Å separation between the O atoms and 3.63–3.78 Å between the out-of-plane H atoms. The isolated water trimer has been investigated experimentally and theoretically by a number of workers [49–56], and is known to have a number of conformers which are close in energy, with the lowest-energy structure being a cyclic asymmetric three OH ring structure having two and one H atoms above and below the ring. We obtain the "crown"-type structure because the electric field from the Al_{19}^- cluster attracts the three dangling OH bonds towards the cluster surface. We compute the isolated crown structure to be only 1 kcal mol^{-1} higher in energy than the asymmetric ring structure. Although the present calculations do not include enough water molecules to allow us to predict the structure for the water layer closest to the cathodic metal surface, they do suggest that the H-bonding network in water is different at the metal interface from that in bulk water. This interface H-bonding network may be the origin of the density increase to 1.55×10^{15} water molecules per cm^2 determined by Toney et al. at the cathodic Ag(111) surface [8]. In our earlier work we determined that water adsorption is preferred at the atop site on the neutral Al(111) surface [23,24]. This suggests for neutral and positively charged Ag(111) surfaces that the water O atom probably has a strong interaction with a particular adsorption site, thereby enabling even closer adsorbate packing so as to produce the higher surface density of 2.6×10^{15} water molecules per cm^2 [8].

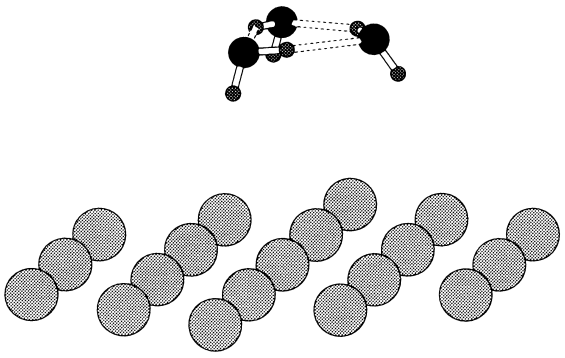

Fig. 4. Optimized structure for a water trimer adsorbed on the Al_{19}^- cluster. The three water molecules readily form a ring of hydrogen bonds with a 2.94 Å separation between the O atoms and a 3.63–3.78 Å separation between the out-of-plane H atoms.

3.2. Adsorption of fluoride and iodide on aluminum clusters

In this section we compare the adsorption interactions taking place between individual fluorine and iodine ions and the cathodic Al(111) surface. To determine the preferred adsorption sites for the two different halides X on the Al(111) surface, we initially performed calculations on the two-layer clusters $Al_{18}(12,6)X^m$ and $Al_{19}(12,7)X^m$, with total charges m equal to -1 and 0. These two cluster types have three central Al surface atoms surrounded by a complete shell of nearest-neighbor Al atoms, and are large enough to enable us to make a comparison between halide adsorption at the atop, bridging and three-fold hollow sites. Both clusters have the same types of atop and bridging adsorption sites, but they differentiate between the two possible types of three-fold sites on the Al(111) surface: the $Al_{18}(12,6)$ cluster has a three-fold hollow fcc site and the $Al_{19}(12,7)$ cluster has a three-fold hollow hcp site. The adsor-

bate equilibrium geometry for a particular site was determined by minimizing the HF cluster energy along the direction normal to the surface site. All of the calculations were performed using C_s point group symmetry. The optimized aluminum–halide distances for the different adsorption sites together with their relative energies E_r and adsorption energies AE computed at both the HF and MP2 levels using the optimized HF geometry are given in Tables 2 and 3. To reduce cluster edge effects, Tables 2 and 3 only include the results for adsorption sites involving the three central surface atoms of the cluster.

Examination of the relative adcluster energies E_r in Tables 2 and 3 shows the halide adsorption at the atop site to be favored in both the SCF and MP2 level calculations for the $Al_{18}(12,6)$ cluster, but only at the SCF level for the $Al_{19}(12,7)$ cluster. The MP2 relative energies for the $Al_{19}(12,7)$ cluster favor fluorine adsorption at the bridge site and

Table 2
Relative total energies E_r (kcal mol^{-1}), adsorption energies AE (kcal mol^{-1}), and optimized geometries (Å) for halide adsorption at different sites on the $Al_{18}(12,6)$ cluster. The halide charge Q_X is from a Löwdin population analysis

Cluster	E_r (HF)	AE (HF)	E_r (MP2)	AE (MP2)	X height	Q_X
Atop site						
$Al_{18}(12,6)F$	0	165	0	171	1.700	−0.87
$Al_{18}(12,6)F^-$	0	101	0	106	1.715	−0.86
$Al_{18}(12,6)I$	0	96	0	113	2.754	−0.50
$Al_{18}(12,6)I^-$	0	36	0	53	2.825	−0.56
Bridge site						
$Al_{18}(12,6)F$	6	161	15	157	1.233	−0.94
$Al_{18}(12,6)F^-$	4	93	21	118	1.305	−0.95
$Al_{18}(12,6)I$	11	85	16	97	2.663	−0.47
$Al_{18}(12,6)I^-$	10	21	26	59	2.828	−0.58
Three-fold fcc site						
$Al_{18}(12,6)F$	7	171	34	182	1.231	−0.97
$Al_{18}(12,6)F^-$	4	109	54	84	1.242	−0.97
$Al_{18}(12,6)I$	11	97	36	122	2.697	−0.49
$Al_{18}(12,6)I^-$	9	37	26	58	2.769	−0.55

Table 3
Relative total energies E_r (kcal mol^{-1}), adsorption energies AE (kcal mol^{-1}), and optimized geometries (Å) for halide adsorption at different sites on the $Al_{19}(12,7)$ cluster. The halide charge Q_X is from a Löwdin population analysis

Cluster	E_r (HF)	AE (HF)	E_r (MP2)	AE (MP2)	X height	Q_X
Atop site						
$Al_{19}(12,7)F$	0	161	0	162	1.700	−0.87
$Al_{19}(12,7)F^-$	0	99	0	101	1.701	−0.87
$Al_{19}(12,7)I$	0	92	0	106	2.748	−0.50
$Al_{19}(12,7)I^-$	0	30	0	49	2.776	−0.55
Bridge site						
$Al_{19}(12,7)F$	4	166	−6	167	1.270	−0.94
$Al_{19}(12,7)F^-$	5	94	−6	107	1.271	−0.94
$Al_{19}(12,7)I$	13	79	4	102	2.748	−0.53
$Al_{19}(12,7)I^-$	9	15	−5	34	3.139	−0.74
Three-fold hcp site						
$Al_{19}(12,7)F$	11	157	15	162	1.216	−0.96
$Al_{19}(12,7)F^-$	18	74	9	72	1.210	−0.96
$Al_{19}(12,7)I$	15	87	23	92	2.740	−0.49
$Al_{19}(12,7)I^-$	11	12	−6	35	3.357	−0.82

iodine at the atop or three-fold hcp site, depending on the cluster total charge. Identification of the preferred adsorption site becomes less clear when one uses the largest halide-ion adsorption energy $AE(X^-)$ defined by Eq. (1). The reason why the adsorption energy results do not mirror the relative energy results is that the required proper bonding states for naked cluster energies change at the different adsorption sites. Interestingly, because each of the adsorption sites may involve a different proper bonding state for the naked cluster, the MP2 *AE*s change by only a small percentage from their HF *AE* values. In contrast, the relative adsorption energies E_r, which do not incorporate any contributions from the naked cluster energies, show at some sites large relative differences between their MP2 and HF E_r values. The relatively small range for the both the E_r and *AE* values listed in Tables 2 and 3 indicates that halide adsorption at the atop, bridge and the two three-fold sites are all close in energy. Although our computed relative energies give the strongest support for halide adsorption at the atop site on Al(111), halide adsorption on the (111) surface of transition metals has usually been found to prefer adsorption at three-fold sites [11,15,20,21]. The reason for this inconsistency is presently unclear, but could be specific to aluminum.

Tables 2 and 3 show that the equilibrium surface–X distances undergo a relatively small increase when the cluster total charge changes from 0 to −1. This suggests the same sort of halide–surface bonding interactions take place regardless of the surface charge. The $Al_{18}(12,6)$ and $Al_{19}(12,7)$ clusters produce very similar halide geometries for the equivalent adsorption sites on both clusters, and only relatively small halide height differences occur between the two types of threefold sites, with the largest changes taking place in the $Al_{19}(12,7)I^-$ clusters. We think this larger I–surface distance at the bridging and three-fold hollow hcp sites on $Al_{19}(12,7)$ is due to an enhanced repulsion between the iodide and the second-layer aluminum atoms, which have an electron negative charge of approximately 0.2.

Although the equilibrium surface–X distances are only slightly affected by changing the cluster charge, the halide adsorption energy $AE(X^-)$ is significantly reduced on going from a neutral cluster to a negatively charged cluster. We find at the HF and MP2 levels that the adsorbate adsorption energies for both the fluoride and iodide ions are reduced by approximately 60 kcal mol^{-1}. The higher halide adsorption energy for the overall neutral cluster is a consequence of the attractive electrostatic interaction between the negatively charged halide ion and the positively charged cluster required by the system charge neutrality. When one tries to model the 60 kcal mol^{-1} adsorption energy jump with an image charge generated inside the Al surface and takes the halide charge as −1, a unit image charge centered approximately 5.5 Å vertically below the halide inside the Al cluster is required. Consideration of this simple image charge model makes it all the more surprising that the surface–X distances are not more sensitive to the total charge of the cluster.

In Tables 2 and 3 we also include estimates of the charges on the halide atoms using a Löwdin population analysis. We find a much larger charge transfer for iodide than for fluoride, which is consistent with the much larger electronegativity of F over I. The fluoride ion remains −1 charged on both the negatively charged and neutral clusters, while the iodide loses almost half an electron to the metal in the neutral clusters and slightly less on the negatively charged clusters. Our results for fluorine are compatible with the conclusions of several other groups on the high ionicity of fluorine atoms adsorbed on metallic surfaces [19,20,48]. Of course, the half-electron charge transfer for I is only approximate due to the well-known uncertainties of population analysis [57].

In Section 3.3 we consider the coadsorption of water and halide on the cathodic Al(111) surface, and it will be convenient to use a cluster with a larger surface area. For this reason we have also performed a series of calculations on differently charged single-layer Al_{19}^m clusters with total charges of $m=-2$, −1 and 0. The advantage of working with the Al_{19}^m cluster is that it is not excessively large for an ab-initio geometry optimization of an adsorbate, even when the cluster has no symmetry. The optimized halide–surface distances, relative energies and adsorption energies on the single-layer Al_{19}^m cluster are given in Table 4 and are in

Table 4
Relative total energies E_r (kcal mol^{-1}), adsorption energies AE (kcal mol^{-1}), and optimized geometries (Å) for halide adsorption at different sites on a single-layer Al_{19} cluster. The halide charge Q_X is from a Löwdin population analysis

Cluster	E_r (HF)	AE (HF)	E_r (MP2)	AE (MP2)	X height	Q_X
Atop site						
$Al_{19}F$	0	156	0	158	1.715	−0.87
$Al_{19}F^-$	0	103	0	98	1.720	−0.87
$Al_{19}F^{-2}$	0	50	0	46	1.722	−0.87
$Al_{19}I$	0	82	0	109	2.839	−0.58
$Al_{19}I^-$	0	32	0	47	2.857	−0.59
$Al_{19}I^{-2}$	0	−19	0	−3	2.869	−0.60
Bridge site						
$Al_{19}F$	11	144	9	149	1.391	−0.95
$Al_{19}F^-$	8	100	26	96	1.409	−0.95
$Al_{19}F^{-2}$	9	42	22	14	1.414	−0.95
$Al_{19}I$	−1	94	39	110	2.711	−0.51
$Al_{19}I^-$	6	37	20	37	2.755	−0.56
$Al_{19}I^{-2}$	2	−21	20	−33	2.800	−0.59
Three-fold site						
$Al_{19}F$	12	154	37	161	1.355	−0.97
$Al_{19}F^-$	11	97	29	91	1.364	−0.97
$Al_{19}F^{-2}$	14	36	18	28	1.379	−0.97
$Al_{19}I$	−1	93	39	110	2.681	−0.50
$Al_{19}I^-$	7	37	23	46	2.714	−0.54
$Al_{19}I^{-2}$	4	−23	15	−18	2.816	−0.61

general similar to the results in Tables 2 and 3 for the Al_{18}(12,6) and Al_{19}(12,7) clusters. The HF and MP2 relative energies E_r again favor halide adsorption at the atop site. Many of the adsorption energies $AE(X^-)$, also prefer halide adsorption at the atop site. As before, the X–surface distances only increase slightly as the cluster charge changes from zero to −2. The jumps in halide adsorption as the Al_{19} cluster are made more negative, and are now approximately 50 kcal mol^{-1} per unit of charge. The slightly smaller change in adsorption energy is consistent with a smaller change in the cluster surface electron charge density owing to the larger surface area as the overall charge of the cluster being increased. Thus, we conclude from Table 4 that single layer Al_{19} can be used as a reasonable model for the Al(111) surface. We will use this cluster in Section 3.3 to model hydrated halide ions on the Al(111) surface.

It is informative to examine the variation of F^- and I^- binding energy with distance above the atop site on the single-layer Al_{19}^q cluster. In Fig. 5 we show F and I adsorption energy curves obtained using the $Al_{19}X^{2-}$ clusters. When the X^- heights are greater than 5 Å the curves become very similar for both ions. This 5 Å height can be considered as the distance where the unique chemical identity of each halide ion disappears and a simple electrostatic interaction between the negatively charged surface and the net ionic charge takes over. The thin dotted line in Fig. 5 is the classical electrostatic energy computed using $E=Vq$, where V is the electrostatic potential calculated by GAMESS using the nuclear positions and electronic wavefunction from the Al_{19}^- cluster, and $q=-1$ is the charge on the halide ion. At large distances, the X^- binding energy for the $Al_{19}X^{2-}$ tends to zero as $1/R$ as the adcluster dissociates into Al_{19}^- and X^-. When X^- approaches the surface, deviation from the $1/R$ binding energy dependence occurs due to additional chemical bonding taking place. The HF and MP2 calculations produce slightly different halide ion adsorption energies but find essentially the same equilibrium vertical height. Similar X^- binding energy curves occur with the $Al_{19}X^-$ clusters, except that the long distance dependence has a zero energy asymptote. Pecina et al. [58] have obtained similarly shaped curves for the

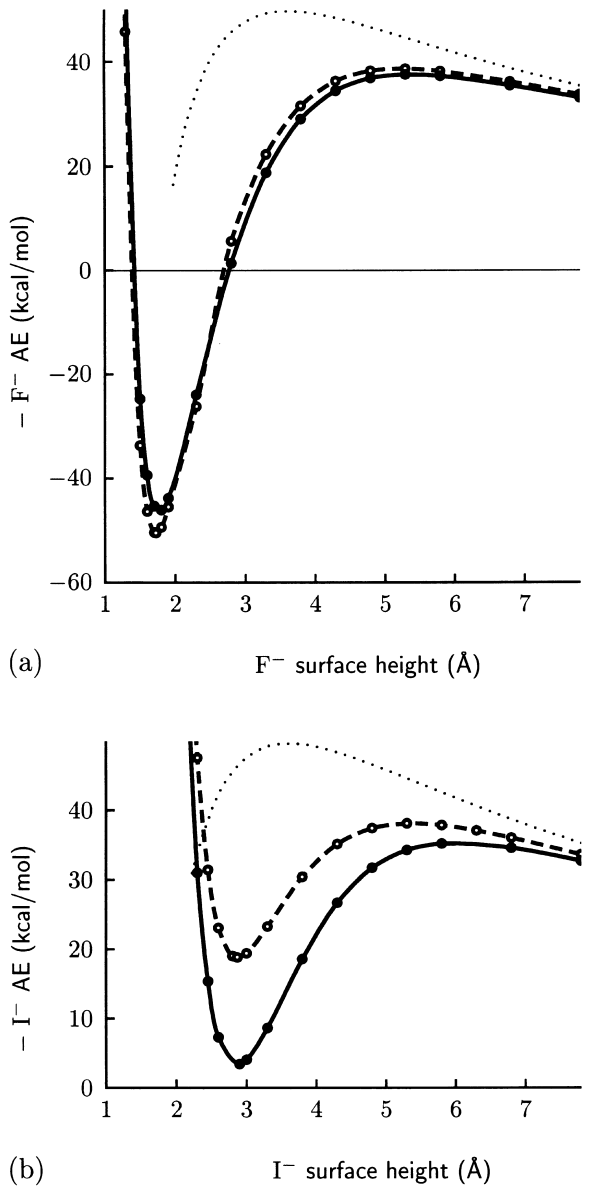

Fig. 5. Variation of the (a) fluoride and (b) iodide ion adsorption energy (HF (○) and MP2 (●)) with vertical distance above the central on-top site in the Al_{19}^- cluster. The dotted line represents an idealized curve of the electrostatic interaction between the bare Al_{19}^- cluster and a negative point charge.

Gibbs energy of the iodide ion in the presence of the electric field near a positively charged surface, using the molecular dynamics calculations for the iodide in the presence of the water molecules. At short X–surface distances, the adsorption energy of the halide deviates strongly from the classical electrostatic energy, suggesting that a strong halide chemisorption interaction takes place. Some evidence for strong halide–Al surface bonding is provided by the contour plots of the total electron density computed for the $Al_{19}X^{-2}$ clusters which show the halide atoms at their equilibrium distances to strongly perturb the Al_{19}^- cluster electron density [47].

At this stage it is tempting to ask whether our calculations can give any insight into why iodide is often found specifically adsorbed on cathodic electrode surfaces while fluoride is not. Consideration of the halide ion adsorption energy alone does not provide a plausible explanation. Our X^- binding energies in Tables 2–4 show that the fluoride always binds much more strongly than iodide to the Al clusters, regardless of the cluster surface charge. The same result for other metal surfaces has been found by previous workers [16–21]. At the MP2 level, Table 4 and Fig. 5 list a F^- binding energy of 46 kcal mol^{-1}, but show I^{-1} to have a negative binding energy of -3 kcal mol^{-1}, indicating that the bound state is less stable than the combined energies of the separate I^- and naked Al_{19}^- in a properly prepared bonding state. However, F^- and I^- do form adsorption states on the Al_{19}^- clusters with fairly deep binding energy wells, and the more important quantity will be the activation energy needed to escape from the well. From Fig. 5 we estimate the MP2 calculated barrier heights are 85 kcal mol^{-1} for F^- and 30 kcal mol^{-1} for I^-. It is worth noting that these barrier heights are only slightly reduced from the halide-ion adsorption energies computed for the neutral Al_{19} clusters and are in agreement with the same type of bonding taking place on both the neutral and the negatively charged Al surfaces. These barrier heights again favor F^- being more strongly specifically adsorbed on a negatively charged electrode than I^-. Obviously, effects due to solvent molecules should also be taken into account. Experiments have shown F^- to have a much larger enthalpy (-113.3 kcal mol^{-1}) of hydration than I^- (-64.1 kcal mol^{-1}) [22], and this extra solvation energy must prevent the F^- from specifically adsorbing on the cathodic electrode surface. We

explore some of the influence exerted by solvent molecules on the halide adsorption in Section 3.3.

3.3. $F^- \cdot H_2O$ and $I^- \cdot H_2O$ adsorption on the Al_{19}^- cluster

The aim of this section is to describe how halide adsorption on the cathodic Al(111) surface is influenced by the coadsorption of water molecules. In a separate study we have recently investigated $F^- \cdot H_2O$ and $I^- \cdot H_2O$ in an external homogeneous electric field [59]. One object of that study was to see whether we could simulate an electrode surface simply with an electric field. While we found some interesting $X^- \cdot H_2O$ geometry changes with increasing electric field strengths, we realized that some account of the chemisorption effects was needed in order to develop a more realistic model for an electrode surface. In this section we approximate the required chemisorption effects using a single-layer Al_{19}^- cluster to simulate the cathodic Al(111) surface. The halide/water geometries were obtained from partial geometry optimization calculations at the HF level keeping the Al cluster atoms at their surface-like positions. Computational limitations prevent us from performing the optimization calculations with a two-layer cluster having the same surface area as the single-layer Al_{19}^- cluster. Unfortunately, the results in Table 1 show that the optimized water height above the Al_{19}^- cluster is slightly longer than those determined for the two-layer clusters. However, as we discuss below, the optimized halide/water geometries we obtain are still able to provide a useful insight into the relative specific adsorption for the F^- and I^- anions.

The geometries found from partial optimizations of $F^- \cdot H_2O$ and $I^- \cdot H_2O$ adsorbed on the Al_{19}^- cluster are shown in Figs. 6 and 7. A summary of the geometric parameters determined for $X^- \cdot H_2O$ adsorbed on Al_{19}^- is given in Table 5, along with the optimized halide to hydrogen distances computed for the isolated $X^- \cdot H_2O$ ions. The isolated $X^- \cdot H_2O$ structures along with their halide–hydrogen distances are in good agreement with results obtained with the more extensive basis sets used in our previous studies [59]. Since the adcluster total energy is minimized while allowing the $X^- \cdot H_2O$ atoms to have unconstrained movement parallel the Al_{19}^- cluster surface, we again find that the halide ion preferentially adsorbs at the atop site. The partially optimized $X^- \cdot H_2O$ structures suggest that the nature of the halide–Al(111) surface interaction is only slightly modified by the presence of the water molecule, since the heights of both the fluoride and the iodide above the cluster surface remain essentially at the same distances as determined previously in the $Al_{19}X^{-2}$ cluster calculations. Furthermore, apart from the I–H bond length increasing by 0.13 Å, the $I^- \cdot H_2O$ optimized geometry on Al_{19}^- is very similar to that computed for the isolated $I^- \cdot H_2O$ ion. The height of the iodide adsorption above the surface enables the water to adopt a geometry which has very little energetic strain from that in the $H_2OAl_{19}^-$ adcluster. In contrast, fluoride adsorption strongly affects the coadsorption of water on the cluster surface. The lower surface height of the adsorbed F^- and the bonding between F^- and water causes the water molecule

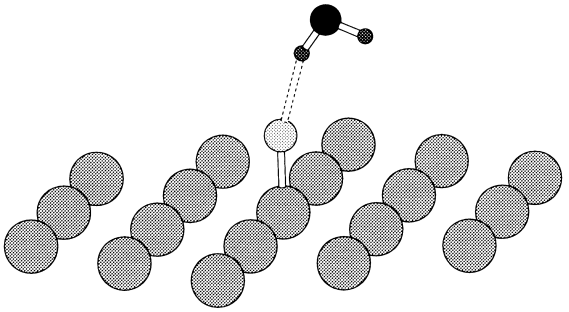

Fig. 6. Optimized $F^- \cdot H_2O$ adsorbed on the Al_{19}^- cluster.

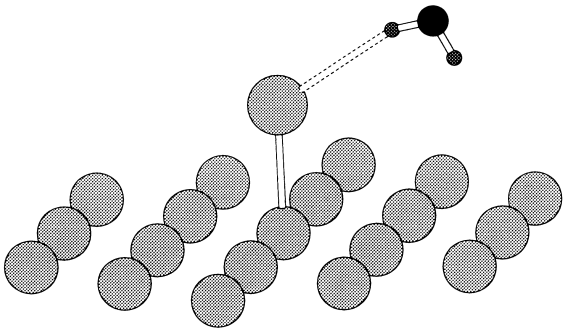

Fig. 7. Optimized $I^- \cdot H_2O$ adsorbed on the Al_{19}^- cluster.

Table 5
Equilibrium geometries (Å) and adsorption energies (kcal mol^{-1}) for $F^- \cdot H_2O$ and $I^- \cdot H_2O$ adsorbed on a single-layer Al_{19}^- cluster. For comparison, the optimized X–H distance in isolated $X^- \cdot H_2O$ along with the water H and X^- vertical heights from the previous Al_{19}^- cluster calculations are included in the table. H_1 labels the water hydrogen atom closest to the halide

Cluster	X height	H_1 height	H_2 height	d (X–H_1)	AE (HF)	AE (MP2)
$F^- \cdot H_2O/Al_{19}^-$	1.74	3.60	3.97	1.96	36	15
$I^- \cdot H_2O/Al_{19}^-$	2.89	4.58	3.92	3.18	−20	−4
H_2O/Al_{19}^-		3.86	3.86			
F^-/Al_{19}^-	1.72				50	46
I^-/Al_{19}^-	2.87				−19	−3
$F^- \cdot H_2O$				1.54		
$I^- \cdot H_2O$				3.05		

to be appreciably pulled towards the Al_{19}^- cluster surface. Instead of the F^-–Al surface bond being stretched, we find a significantly longer F–H distance of 1.96 Å in the adsorbed $F^- \cdot H_2O$ relative to the equilibrium 1.54 Å F–H distance computed for the isolated $F^- \cdot H_2O$. Even with F–H bond stretching, the water H_1 atom which bonds to the F^- is still only 3.60 Å above the cluster surface, and is approximately 0.26 Å closer to the surface than determined for the $H_2OAl_{19}^-$ adcluster. Interestingly, the second water hydrogen has a surface height similar to that found for the $I^- \cdot H_2O$ case. One measure of how F^- adsorption is more strongly affected than I^- by hydration is provided by the $X^- \cdot H_2O$ adsorption energy $AE(X^- \cdot H_2O)$ defined by Eq. (1). The $X^- \cdot H_2O$ adsorption energies are listed in Table 5. To illustrate the effect of hydration we also include in Table 5 the X^- adsorption energies at the atop sites on the Al_{19}^- cluster originally listed in Table 4. As expected, since the chemisorbed $I^- \cdot H_2O$ structure closely resembles the isolated $I^- \cdot H_2O$ structure and has the water molecule at a height greater than in the optimized $Al_{19} \cdot H_2O^-$ cluster, the $I^- \cdot H_2O$ adsorption energy is only 1 kcal mol^{-1} less than the I^- adsorption energy. In contrast, the longer F–H distance and lower water–surface height for chemisorbed $F^- \cdot H_2O$ reduces the $F^- \cdot H_2O$ adsorption energy by 14 kcal mol^{-1} relative to the F^- adsorption energy. A structure with a shorter F–H distance, which is closer to that in isolated $F^- \cdot H_2O$, should help to stabilize the $F^- \cdot H_2O$ adsorption energy, although the shorter F–H distance would pull the H_2O even closer to the surface and thereby further destabilize the $F^- \cdot H_2O$ adsorption energy. Unfortunately, the hydrogen heights on the single-layer Al_{19}^- cluster are 0.13 Å longer than on the two-layer clusters listed in Table 1. Thus, we might anticipate finding a smaller difference between the $F^- \cdot H_2O$ and the F^- adsorption energies on the two-layer $Al_{31}(19,12)^-$ cluster.

Nonetheless, the present $X^- \cdot H_2O/Al_{19}^-$ calculations suggest the following microscopic explanation as to why the I^- anion specifically adsorbs on a cathodic electrode whereas F^- does not. The hydrated fluoride ion, when adsorbed on the metal surface, will have long F—H bonds with the water molecules. The short F–Al surface distance requires the water molecules which form F—H bonds to be pulled into the region of the steeply increasing water–surface repulsion "wall" for the Al(111) surface shown in Fig. 3 at around 3 Å. When the F^- ion is adsorbed on the Al(111) surface, it has penetrated deeply inside the zone forbidden for the water. The halide heights given in Tables 3–5 show that F^- adsorption at bridge or three-fold sites would be even deeper in the forbidden zone. Presumably, the hydration of F^- is more energetically favorable than the adsorption of F^- adsorption on the Al(111) surface, and as a consequence F^- does not specifically adsorb on the cathodic surface. Hydration of I^- is also probably favored over I^- adsorption on the cathodic Al(111) surface. However, the chemisorbed $I^- \cdot H_2O$ structure shown in Fig. 7 suggests that the I^- adsorption height and the I—H bond lengths are large enough that water molecules are

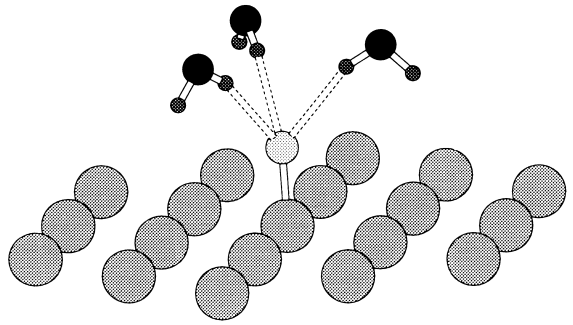

Fig. 8. The optimized $F^- \cdot (H_2O)_3$ structure on Al_{19}^- obtained using a C_{3v} symmetry constraint.

still able to bond with I^- without having to penetrate the repulsive water–surface wall. Thus, iodide is able to be specifically adsorbed on the cathodic Al(111) surface while preserving hydration effects.

The presence of more water molecules in the calculations might be expected to detach the F^- ion from the Al_{19}^- cluster surface. To investigate this, we partially optimized $X^- \cdot (H_2O)_3$ adsorbed on Al_{19}^-, initially using C_{3v} symmetry to simplify the calculations. The resulting C_{3v} structures are shown in Figs. 8 and 9, with the most important equilibrium geometry parameters being given in Table 6. In agreement with the discussion of the previous paragraph, the partially optimized $I^- \cdot (H_2O)_3$ adsorbate has an I^- surface height, H–I distances and water heights above the Al_{19}^- cluster which are very similar to those computed for the $I^- \cdot H_2O$ adsorption. Further confirmation that the $I^- \cdot (H_2O)_3$ structure is not strained is given by the adsorption energy, computed using Eq. (1), being only 5 kcal mol^{-1} higher than the I^- adsorption energy. However, the partial geometry optimization for $F^-(H_2O)_3$ adsorption does not produce any evidence for the three water molecules causing F^- to become detached from the surface, since there is only a slight increase in the fluoride adsorption height. Nonetheless, the adsorbed structure is obviously strained, since with C_{3v} symmetry we find that the F—H bonds are stretched to 2.43 Å from the 1.96 Å computed for adsorbed $F^- \cdot H_2O$. Even with these longer F—H bonds, the three water molecules are closer to the Al_{19}^- cluster surface than in the $F^- \cdot H_2O/Al_{19}^-$ structure, and this is probably due to repulsion between the water molecules. The adsorption energy for the C_{3v} $F^- \cdot (H_2O)_3$ structure is raised by 41 kcal mol^{-1} above the adsorption energy for F^-alone. Some of the repulsion between the water molecules is reduced when the $F^- \cdot (H_2O)_3$ partial optimization is performed with lower C_3 symmetry. The optimized crown-like C_3 structure for $F^- \cdot (H_2O)_3$ is shown in Fig. 10, and is 7 kcal mol^{-1} more stable than the C_{3v} structure. The slightly larger H′FH″ angle between two water molecules in the C_3 structure correlates with reducing the water–water repulsion, but this angle is still significantly more acute than that determined for $I^- \cdot (H_2O)_3$ adsorption. The C_3 structure for $F^- \cdot (H_2O)_3$ is destabilized by forming long 2.72 Å F—H bonds, but this is compensated by the water molecules being at a greater height above the Al_{19}^- surface and by the formation of hydrogen

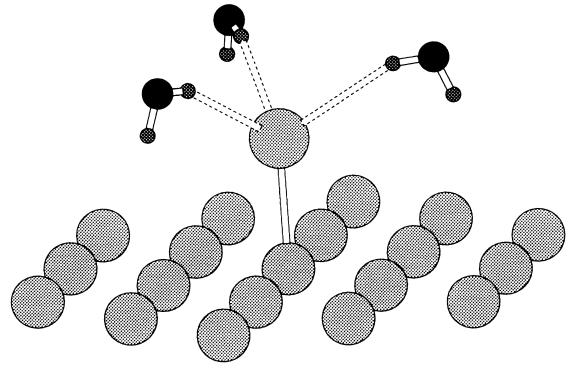

Fig. 9. The optimized $I^- \cdot (H_2O)_3$ structure on Al_{19}^- obtained with both the C_{3v} and the C_3 symmetry constraints.

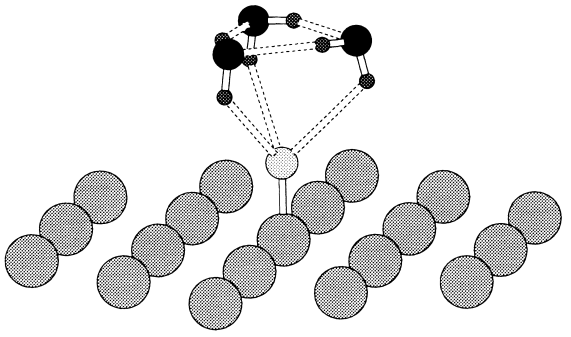

Fig. 10. The optimized $F^- \cdot (H_2O)_3$ structure on Al_{19}^- obtained when the C_{3v} constraint is relaxed to C_3 symmetry.

Table 6
Equilibrium geometries (Å) and adsorption energies (kcal mol^{-1}) for $F(H_2O)_3^-$ and $I(H_2O)_3^-$ adsorbed on the single-layer Al_{19}^- cluster. The HF *AE*s are listed first, followed by the MP2 *AE*s in parentheses

Cluster	Symmetry	X height	H_1 height	H_2 height	d(X–H_1)	H_1'–$\hat{X}$–H_1'' (deg.)	*AE*
$F(H_2O)_3^-/Al_{19}^-$	C_{3v}	1.77	3.46	3.61	2.43	69	9 (4)
$F(H_2O)_3^-/Al_{19}^-$	C_3	1.75	3.66	4.66	2.72	76	16 (14)
$I(H_2O)_3^-/Al_{19}^-$	C_{3v}, C_3	2.97	4.68	3.96	3.20	94	−24 (−12)

bonds between the water molecules. When performing an $I^- \cdot (H_2O)$ partial geometry optimization starting with a structure having C_3 symmetry, the optimization converges back to the same C_{3v} structure, as discussed above. The optimized C_{3v} $I^- \cdot (H_2O)_3$ geometry is consistent with the iodide being both specifically adsorbed on a surface and being hydrated at the same time. Although the $F^- \cdot (H_2O)_3$ calculations show that the three water molecules on their own are not capable of detaching F^- from the Al surface, presumably in an electrolyte above an electrode there will be a more extensive hydrogen-bonded network of water molecules which are able to provide the force necessary to completely break the fluoride–surface bond.

4. Conclusions

By performing ab-initio calculations on several different negatively charged Al clusters, we can make the following semi-quantitative conclusions about water, fluorine and iodine adsorption on the negatively charged Al(111) surface.

(1) In agreement with in situ experiments on electrode surfaces and simple electrostatic considerations, we find that water adsorbs with the hydrogen atoms closest to the cathodic surface. The direction of the water molecule is reversed to that found in the adsorption of water on neutral Al clusters. However, the water adsorption is weak and appears to be mostly due to the water dipole moment interacting with the surface electric field. The water does not have a strong site preference and is at a distance from the cathodic Al(111) surface which is about 1.5 times longer than found for the neutral surface. A steep repulsive interaction develops when the water is within ~3.0 Å of the surface. In the cluster calculations with multiple water molecules, we find that a H-bond network is formed between the water molecules. This H-bonding network might be different to that which occurs in bulk water, and may be responsible for the increase in water density at a cathodic electrode recently observed by in situ surface X-ray scattering experiments [8].

(2) F^- binds much more strongly than I^- to the Al(111) surface. The relative energies for different adsorption sites on the same cluster suggest that F^- and I^- adsorption is preferred at the atop sites. However, halide adsorption energies, computed using Eq. (1) with appropriate prepared state energies for the bare clusters, make the identification of the preferred adsorption site less certain. The halide ion adsorption energy decreases with increasing cluster charge. Both the F^- and I^- adsorption energy decreases by 50 kcal mol^{-1} for each electron charge increment. F^- has a positive adsorption energy and is still bound to Al_{19}^- in the $Al_{19}F^{2-}$ cluster, whereas $Al_{19}I^{2-}$ is unstable relative to Al_{19}^- and I^-, but there is a 30 kcal mol^{-1} activation energy to separation. We compute a 85 kcal mol^{-1} activation energy for F^- desorption from the $Al_{19}F^{2-}$ cluster.

(3) In the presence of water, the F^- and I^- ions adsorb at atop sites on the Al_{19}^- clusters with essentially the same vertical heights as when water is absent. The shorter vertical height of F^- results in the Al—F bond being strained by the coadsorption of water. When the coadsorbed water molecule H bonds to a chemisorbed F^-, the Al—F bond is destabilized because the F^- pulls the water molecule too close to the cathodic Al(111) surface and induces a repulsive interaction. At the HF level, the Al—F bond strain amounts to

14 kcal mol^{-1} for the first water molecule and 34 kcal mol^{-1} for three water molecules. Since I^- has a much greater vertical height, the chemisorbed $I^- \cdot H_2O$ is able to maintain a structure on the Al_{19}^- cluster similar to that for isolated $I^- \cdot H_2O$, and the I—Al bond remains unstrained. Thus, I^- is able to specifically adsorb on the cathodic Al(111) surface while maintaining solvation types of interactions with water. In contrast, even though F^- forms a much stronger bond with the cathodic Al(111) surface than I^-, solvation effects destabilise the Al—F bond. Presumably, it is these solvation effects which prevent F^- from specifically adsorbing on the cathodic Al(111) surface.

Acknowledgements

We are grateful for the generous use of the IBM SP2 computer at the Maui High Performance Computing Center.

References

[1] P.A. Thiel, T.E. Madey, Surf. Sci. Rep. 7 (1987) 211.
[2] G. Pirug, H.P. Bonzel, in: J. Lipkowski, P.N. Ross (Eds.), Structure of Electrified Interfaces, VCH, New York, 1993, ch. 5.
[3] M.R. Philpott, J.N. Glosli, in: H.L. Sellers, J.T. Golab (Eds.), Theoretical and Computational Approaches to Interface Phenomena, Plenum, New York, 1994, p. 75.
[4] K. Heinzinger, in: J. Lipkowski, P.N. Ross (Eds.), Structure of Electrified Interfaces, VCH, New York, 1993, ch. 7.
[5] M.R. Philpott, J.N. Glosli, ACS Symp. Ser. 656 (1997) 13.
[6] E. Spohr, ACS Symp. Ser. 656 (1997) 31.
[7] K.J. Schweighofer, X. Xia, M.L. Berkowitz, Langmuir 12 (1996) 3747.
[8] M.F. Toney, J.N. Howard, J. Richer, G.L. Borges, J.G. Gordon, O.R. Melroy, D.G. Weisler, D. Yee, L.B. Sorensen, Nature 368 (1994) 444, Surf. Sci. 335 (1995) 326.
[9] K. Ataka, T. Yotsuyanagi, M. Osawa, J. Phys. Chem. 100 (1996) 10664, Langmuir 14 (1998) 951.
[10] M.A. Habib, J.O'M. Bockris, in: J.O'M. Bockris, B.E. Conway, E. Yeager (Eds.), Comprehensive Treatise of Electrochemistry, vol. 1, Plenum, New York, 1980, ch. 4.
[11] D.D. Sneddon, A.A. Gewirth, Surf. Sci. 343 (1995) 185.
[12] X. Gao, M.J. Weaver, J. Am. Chem. Soc. 114 (1992) 8544.
[13] H. Haiss, J.K. Sass, X. Gao, M.J. Weaver, Surf. Sci. 274 (1992) L253.
[14] S. Yau, C.M. Vitus, B.C. Schardt, J. Am. Chem. Soc. 112 (1990) 3677.
[15] R.G. Jones, Prog. Surf. Sci. 27 (1988) 25.
[16] F. Illas, J. Rubio, J.M. Ricart, J.A. Garrido, J. Electroanal. Chem. 200 (1989) 47.
[17] M. Blanco, J. Rubio, F. Illas, J. Electroanal. Chem. 261 (1989) 39.
[18] M. Blanco, J.M. Ricart, J. Rubio, F. Illas, J. Electroanal. Chem. 267 (1989) 243.
[19] P.S. Bagus, G. Pacchioni, M.R. Philpott, J. Chem. Phys. 90 (1989) 4287.
[20] G. Pacchioni, Electrochim. Acta 41 (1996) 2285.
[21] A. Ignaczak, J.A.N.F. Gomes, J. Electroanal. Chem 420 (1997) 71.
[22] H.L. Friedman, C.V. Krishnan, in: F. Franks (Ed.), Water, a Comprehensive Treatment, vol. 3, Plenum, London, 1973, ch. 1.
[23] S. Jin, J.D. Head, Surf. Sci. 318 (1994) 204.
[24] M.D. Calvin, J.D. Head, S. Jin, Surf. Sci. 345 (1996) 161.
[25] G. Pacchioni, P.S. Bagus, F. Parmigiani (Eds.), Cluster Models for Surface and Bulk Phenomena, Plenum, New York, 1992.
[26] J.L. Whitten, H. Yang, Surf. Sci. Rep. 24 (1996) 55.
[27] H. Sellers, P.V. Sudhakar, J. Chem. Phys. 97 (1992) 6644.
[28] R.R. Nazmutdinov, M. Probst, K. Heinzinger, J. Electroanal. Chem. 369 (1994) 227.
[29] H. Yang, J.L. Whitten, Surf. Sci. 223 (1989) 131.
[30] P.S. Bagus, C.J. Nelin, W. Müler, M.R. Philpott, H. Seki, Phys. Rev. Lett. 58 (1987) 559.
[31] CRC Handbook of Chemistry and Physics, 71st ed., CRC Press, Boca Raton, FL, 1990.
[32] P.J. Knowles, J.S. Andrews, R.D. Amos, N.C. Handy, J.A. Pople, Chem. Phys. Lett. 186 (1991) 130.
[33] W.J. Lauderdale, J.F. Stanton, J. Gauss, J.D. Watts, R.J. Bartlett, Chem. Phys. Lett. 187 (1991) 21.
[34] J.D. Head, J. Comput. Chem 11 (1990) 67.
[35] M.W. Schmidt, K.K. Baldridge, J.A. Boatz, S.T. Elbert, M.S. Gordon, J.H. Jensen, S. Koseki, N. Matsunaga, K.A. Nguyen, S. Su, T.L. Windus, M. Dupuis, J.A. Montgomery Jr., J. Comput. Chem 14 (1993) 1347.
[36] P.J. Hay, W.R. Wadt, J. Chem. Phys. 82 (1985) 284.
[37] T.H. Dunning Jr., P.J. Hay, in: H.F. Schaefer III (Ed.), Modern Theoretical Chemistry, vol. 3, Plenum, New York, 1977, p. 1.
[38] GAMESS User Guide, Iowa State University, 1996.
[39] I. Panas, J. Schule, P.E.M. Siegbahn, U. Wahlgren, Chem. Phys. Lett. 149 (1988) 265.
[40] I. Panas, P.E.M. Siegbahn, J. Chem. Phys. 92 (1990) 4625.
[41] P.E.M. Siegbahn, L.G.M. Pettersson, U. Wahlgren, J. Chem. Phys. 94 (1991) 4024.
[42] P.E.M. Siegbahn, U. Wahlgren, Int. J. Quantum Chem. 42 (1992) 1149.
[43] J. Seitz-Beywl, M. Poxleitner, M.M. Probst, K. Heinzinger, Int. J. Quantum Chem. 42 (1992) 1141.
[44] An.M. Kuznetsov, Electrochim. Acta 40 (1995) 2485.
[45] J. Emsley, The Elements, 2nd ed., Clarendon Press, Oxford, 1995.

[46] S.F. Boys, F. Bernadi, Mol. Phys. 19 (1970) 553.
[47] V. Kairys, Ph.D. Dissertation, University of Hawaii, 1997.
[48] P.S. Bagus, G. Pacchioni, C.J. Nelin, in: R. Carbo (Ed.), Studies in Physica and Theoretical Chemistry, vol. 62, Elsevier, Amsterdam, 1989, p. 475.
[49] N. Pugliano, J. Saykally, Science 257 (1937) 1992.
[50] G.C.M. van Duijneveldt-van de Rijdt, F.B. van Duijneveldt, Chem. Phys. 175 (1993) 271.
[51] S.S. Xantheas, T.H. Dunning Jr., J. Chem. Phys. 98 (1993) 8037.
[52] J.E. Fowler, H.F. Schaefer III,, J. Am. Chem. Soc. 117 (1995) 446.
[53] D.A. Estrin, L. Paglieri, G. Corongiu, E. Clementi, J. Phys. Chem. 100 (1996) 8701.
[54] J. Ortega, J.P. Lewis, O.P. Sankey, Phys. Rev. B 50 (1994) 10516.
[55] D.J. Wales, J. Am. Chem. Soc. 115 (1993) 11180.
[56] T.R. Walsh, D.J. Wales, J. Chem. Soc., Faraday Trans. 92 (1996) 2505.
[57] P.S. Bagus, K. Hermann, C.W. Bauschlicher, J. Chem. Phys. 81 (1966) 1984.
[58] O. Pecina, W. Schmickler, E. Spohr, J. Electroanal. Chem. 394 (1995) 29.
[59] V. Kairys, J.D. Head, J. Phys. Chem. A 102 (1998) 1365.